Supporting Information

Neomangiferin defect-engineering ZIF-8 for visual differentiating aprotic/protic solvents and real-time sensing trace water

Chaoying Tong,[a] Guihan Cai,[a] Yahui Yang,[b] Tongtao Wang,[a] Yangyu Yang,[a] Yuxia Chen,[a] Shuyun Shi,*[abc] Linlin Wu*[a] and Ying Guo*[c]

[a]College of Chemistry and Chemical Engineering, Central South University, Changsha 410083, China

[b]Key Laboratory of Chemical Biology and Traditional Chinese Medicine Research (Ministry of Education of China), Hunan Normal University, Changsha 410081, China

[c]Department of Clinical Pharmacology, Xiangya Hospital, Hunan Key Laboratory of Pharmacogenetics, Central South University, Changsha 410078, China

*Corresponding authors. Tel.: +86 731 88879616.

E-mail addresses: shuyshi@csu.edu.cn (S. Shi); chemwll@csu.edu.cn (L. Wu); guoying881212@csu.edu.cn (Y. Guo)

1. Materials and apparatus

All the used reagents are of analytical grade. Methanol (MeOH), ethanol (EtOH), *n*-butyl alcohol (*n*-BuOH), dimethylsulfoxide (DMSO), dichloromethane (CH_2Cl_2), ethyl acetate (EA), tetrahydrofuran (THF), dioxane, and *n*-hexane (*n*-hex) were purchased from Sinopharm Chemical Reagent Co., Ltd. (Beijing, China), which were further dried with 4 Å molecular sieves for 24 h before use. Zinc nitrate hexahydrate ($Zn(NO_3)_2 \cdot 6H_2O$, 98%), 2-methylimidazole (MIM, 98%) and acetonitrile-d3 (CD_3CN, ≥ 99.8 atom %D) were bought from Sigma-Aldrich (Shanghai, China). Lithium chloride (LiCl), potassium acetate (CH_3COOK), magnesium chloride hexahydrate ($MgCl_2 \cdot 6H_2O$), potassium carbonate crystal ($K_2CO_3 \cdot 2H_2O$), sodium bromide (NaBr) with purity over 99.0% were obtained from Aladdin (Shanghai, China). CO_2, N_2, CO, H_2, CH_4, O_2, C_2H_6, C_2H_4, and C_2H_2 were provided by Guangzhou Xizhou Gas Co., Ltd. (Guangzhou, China). Ultrapure water (18.2 M Ω•cm) was prepared by Milli-Q water purification system (Millipore, Bedford, MA, USA). Neomangiferin (purity > 98%) was provided by Chengdu Purechem-standard Co., Ltd. (Chengdu, China).

UV-vis spectra were collected on UV-2600 UV-vis spectrophotometer (Shimadzu, Japan). Fluorescence spectra were recorded by Perkin-Elmer LS-55 luminescence spectrometer (PerkinElmer, USA). Fluorescent signal was recorded under an excitation wavelength at 348 nm, and the spectra were collected between 400–700 nm. Excitation slit and emission slit were set at 10.0 and 15.0 nm. Differential scanning calorimetry-thermogravimetric (DSC-TGA) analysis (heating rate, 10 °C min^{-1}) was performed on SDT Q600 V7.0 Build 84 thermal analyzer (TA Instruments, USA). Fourier transform infrared spectroscopy (FT-IR) were measured by Spectrum Two (PerkinElmer Ltd., USA). Brunauer-Emmett-Teller (BET) specific surface area and pore volume were tested by N_2 adsorption-desorption experiments on Kubo X1000 (Beijing BUILDER

electronic technology CO., Ltd, China). Scanning electron microscopy (SEM) images were taken by JSM-7610FPlus field-emission scanning electron microscope (JEOL, Japan). Power X-ray powder diffraction (PXRD) characterizations were conducted with SMART APEXII (Bruker, Germany). X-ray photoelectron spectroscopy (XPS) detection was carried out on Thermo Scientific K-Alpha (Thermo Fisher Scientific, USA). Fluorescence lifetimes and absolute quantum yield of neomangiferin-ZIF-8 in different solvents were confirmed by FLS1000 Photoluminescence Spectrometer (Edinburgh Instruments, England). The acid site of neomangiferin-ZIF-8 was measured through CD_3CN adsorption following with FT-IR on a Thermo Fisher Nicolet iS50 (Thermo Fisher Scientific, USA).

Table S1. Reported MOF-based fluorescent sensors for H_2O detection.

NO.	Sensor[a]	Linear range[b] (%, *v*/*v*)	LOD (%, *v*/*v*)	Response time	Solvatochromism	Reversible RH sensing	Sensing mechanism[d]	Ref.
1	Eu^{3+}@UiO-66-NH_2	EtOH, 0.0–2.0 DMF, 0.0–2.0	0.088 0.054	10 min	No	–[c]	Water quenching effect on Eu^{3+}	1
2	Eu-DPA/PTA-NH_2	EtOH, 0.0−100.0	0.01	20 s	No	–	(1) ICT effect of ligands (2) Water quenching effect on Eu^{3+}	2
3	R6G@Eu-MOF	DMSO, 0−4.0 DMF, 0.0−12.4 ACN, 0.0−10.0 THF, 0.0−1.8 MeOH, 0.0−3.5 EtOH, 0.0−1.0 IPA, 0.0−0.8 *n*-BuOH, 0−0.4	0.046 0.085 0.094 0.032 0.032 0.028 0.016 0.021	70 s	No	–	(1) Water induced release of R6G (2) Water quenching effect on Eu^{3+}	3
4	$[Eu(atpt)_{1.5}(H_2O)]_n$	DMF, 0.05−6.0	0.02	–	Yes	–	ICT of ligand	4
5	Eu-MOF	THF, 0.000−0.075	0.0003	< 30 s	No	Yes	Water quenching effect on Eu^{3+}	5
6	Eu-MOFs/CDs	EtOH, 0.05−4.0	0.03	–	No	–	(1) Water quenching effect on Eu^{3+} (2) Aggregation-induced quenching of CDs	6
7	Ru@MIL–NH_2	EtOH, 0.0−100.0	0.02	10 s	No	–	Protonation of ligand	7
8	Zr-MOF	–	–	24 h	Yes	–	Water induced ligand twisting	8
9	Zn-MOF	MeOH, 0.0–1.3% EtOH, 0.0–0.7% Acetone,0.00–0.25% ACN, 0.00–0.15%	–	~2 s	No	Yes	ESIPT of ligand	9

		THF, 0.00–0.40% DMF, 0.00–1.33%						
10	Mg-MOF	–	–	1–2 min	Yes	–	Higher affinity of water with MOF	10
11	QG-loaded MOF	EtOH, 0.05−6.0 DMF, 0.10−9.5	0.015 0.03	–	No	–	Framework collapse	11
12	Mn-MOF	DMSO, 0.0−10.0 MeOH, 0.0−2.5 EtOH, 0.0−7.5 IPA, 0.05−5.0 Acetone, 0.05−2.5 DMF, 0.0−6.25	0.04 0.11 0.16 0.05 0.09 0.18	2 min	No	–	(1) Water-induced ligand exchange (2) Framework collapse	12
13	AIEgen-MOF	–	–	24 h	No	Yes	AIE	13
14	Neomangiferin-ZIF-8	Dioxane, 0.05−5.00 THF, 0.05−3.00 DMSO, 0.50−40.00 EtOH, 0.50−20.00 MeOH, 0.50−10.00	0.01 0.02 0.27 0.30 0.21	8 s	Yes	Yes	LLCT	**This work**

[a]Eu-DPA/PTA-NH_2, Eu-dipicolinic acid/2-aminophthalic acid; R6G@Eu-MOF, Rhodamine 6G@[Eu-(1,4-terephthalic acid)$_{1.5}$(1,10-phenanthroline)(H_2O)]$_n$ MOF; atpt, 2-aminoterephthalic acid; CDs, carbon dots; QG, Q-graphene; AIE, aggregation induced enhancement;

[b]DMF, Dimethyl formamide; ACN, acetonitrile; IPA, isopropanol;

[c]Not mentioned;

[d]ICT, Intramolecular charge transfer.

References

1 S. Y. Zhu and B. Yan, *Ind. Eng. Chem. Res.*, 2018, **57**, 16564–16571.

2 L. Yu, Q. Zheng, H. Wang, C. Liu, X. Huang and Y. Xiao, *Anal. Chem.*, 2020, **92**, 1402–1408.

3 J. Li, P. Du, J. Chen, S. Huo, Z. Han, Y. Deng, Y. Chen and X. Lu, *Anal. Chem.*, 2020, **92**, 8974–8982.

4 Y. Zhou, D. Zhang, W. Xing, J. Cuan, Y. Hu, Y. Cao and N. Gan, *Anal. Chem.*, 2019, **91**, 4845−4851.

5 W. Zhang, J. Xie, Z. Sui, Z. Xu, X. Wang, M. Lei, H. Zhang, Z. Li, Y. Wang, W. Liu, W. Du and S. Wang, *Sci. China Chem.*, 2021, **64**, 1723−1729.

6 Y. Dong, J. Cai, Q. Fang, X. You and Y. Chi, *Anal. Chem.*, 2016, **88**, 1748−1752.

7 H. Q. Yin, J. C. Yang and X. B. Yin, *Anal. Chem.*, 2017, **89**, 13434−13440.

8 R. J. Marshall, Y. Kalinovskyy, S. L. Griffin, C. Wilson, B. A. Blight and R. S. Forgan, *J. Am. Chem. Soc.*, 2017, **139**, 6253−6260.

9 L. Chen, J. W. Ye, H. P. Wang, M. Pei, S. Y. Yin, Z. W. Wei, L. Y. Zhang, K. Wu, Y. N. Fan and C. Y. Su, *Nat. Commun.*, 2017, **8**, 15985.

10 A. Douvali, A. C. Tsipis, S. V. Eliseeva, S. Petoud, G. S. Papaefstathiou, C. D. Malliakas, I. Papadas, G. S. Armatas, I. Margiolaki, M. G. Kanatzidis, T. Lazarides and M. J. Manos, *Angew. Chem. Int. Ed.*, 2015, **54**, 1651−1656.

11 Y. Cai, L. Feng, Y. Hua, H. Liu, M. Yin, X. Lv, S. Li and H. Wang, *Chem. Commun.*, 2018, **54**, 13595−13598.

12 K. Yu, G. Zhang, H. Chai, L. Qu, D. Shan and X. Zhang, *Sens. Actuators B: Chem.*, 2022, **362**, 131808.

13 F. Tan, L. Zha and Q. Zhou, *Adv. Mater.*, 2022, **34**, 2201470.

Fig. S1. Scheme (A) and photographs (B) of lab-made device for RH sensing.

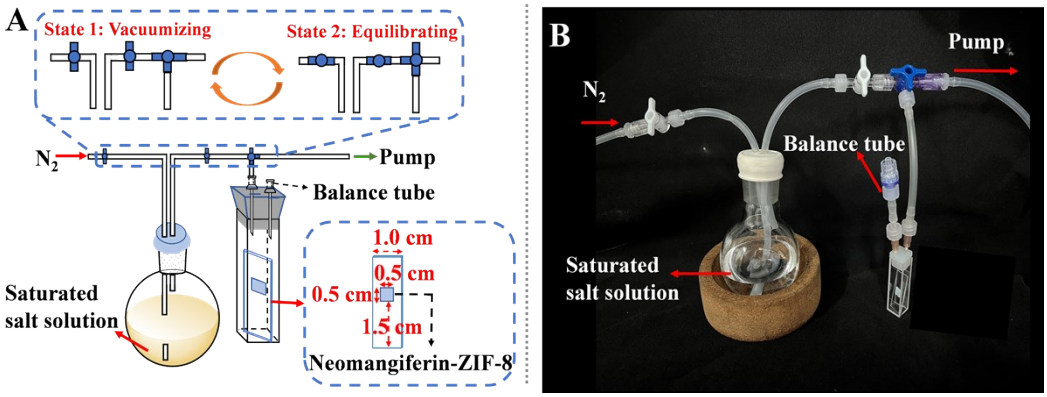

Fig. S2. SEM image of ZIF-8 (Inset is the corresponding particle size distribution diagram).

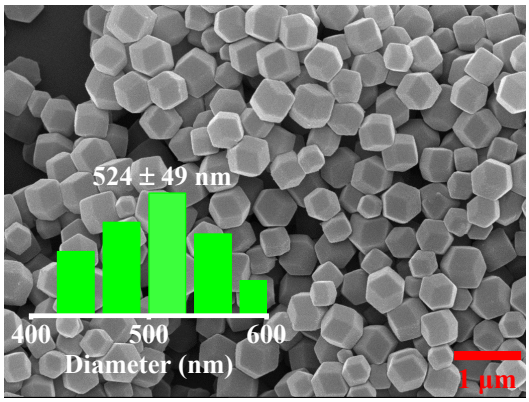

Fig. S3. (A) Nitrogen adsorption-desorption isotherms of neomangiferin-ZIF-8 and ZIF-8; (B) FT-IR spectra of neomangiferin-ZIF-8 and ZIF-8 before and after CD_3CN absorption.

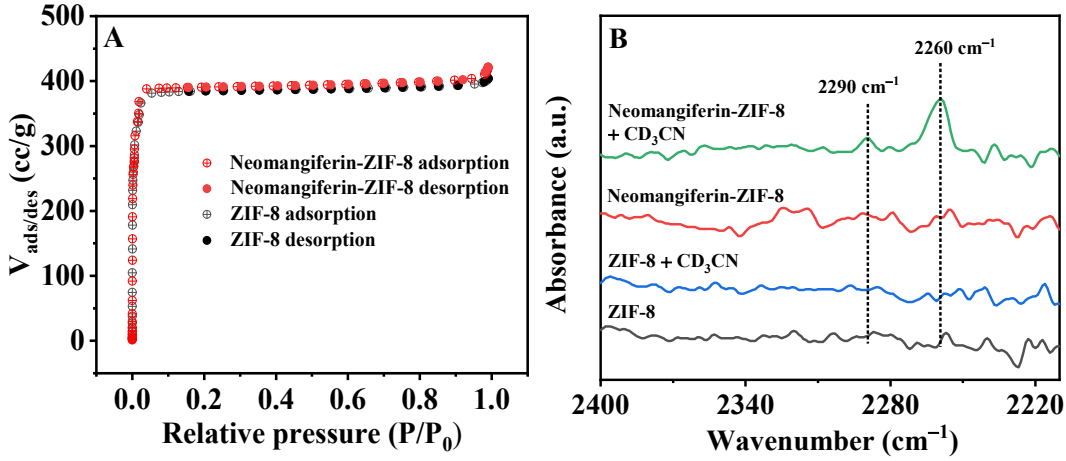

Fig. S4. Full scan XPS spectra of ZIF-8 (A), neomangiferin (B), and neomangiferin-ZIF-8 (C) and high resolution XPS spectra of O1s for ZIF-8 (D), neomangiferin (E), and neomangiferin-ZIF-8 (F).

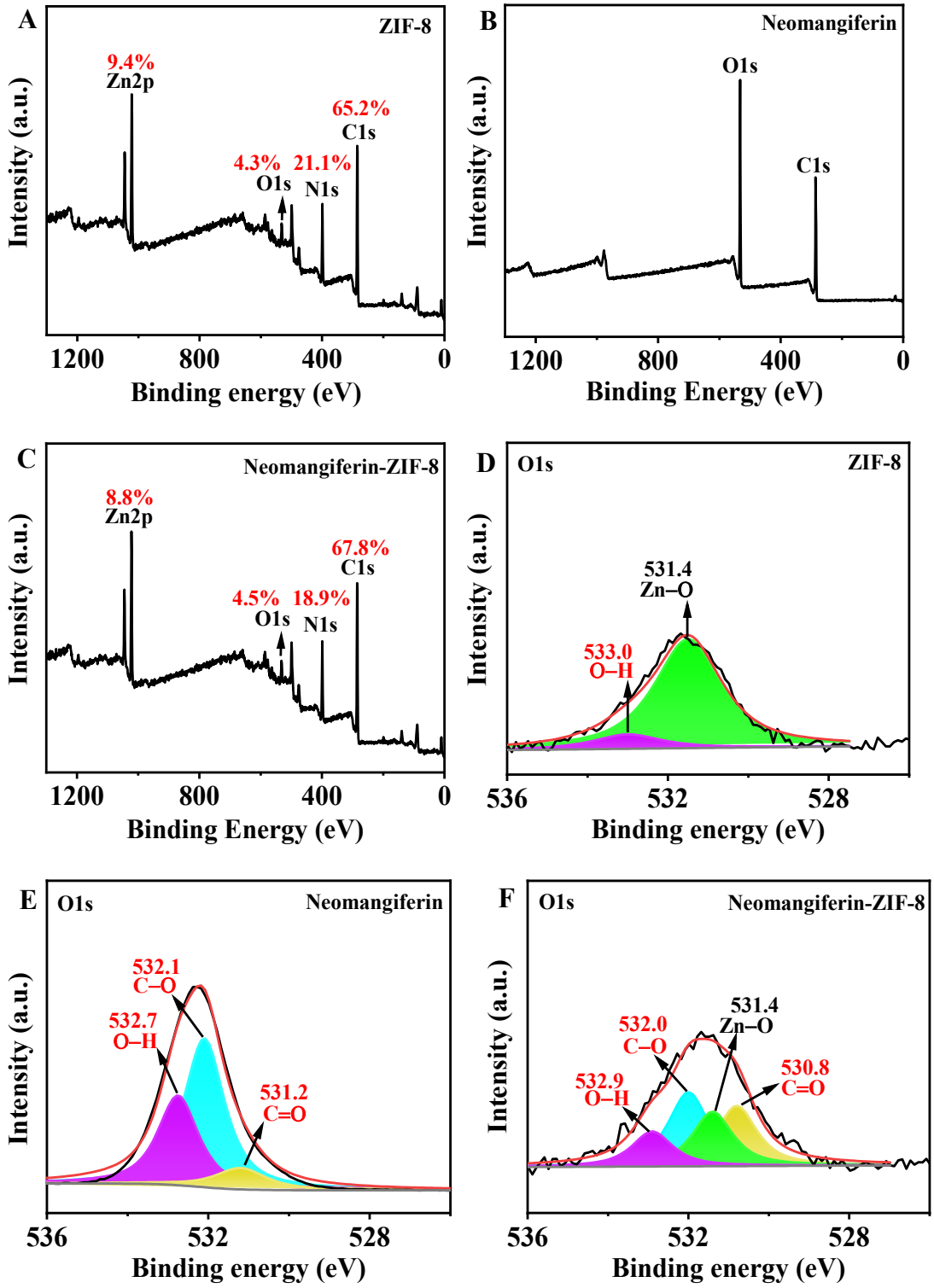

For ZIF-8, C1s, N1s, O1s, and Zn2p are located at 284.7, 398.8, 531.6, and 1021.8

eV with atomic percentages of 65.2%, 21.1%, 4.3% and 9.4%.

For neomangiferin, C1s, and O1s are located at 285.8 and 532.3 eV with atomic percentages of 63.2% and 36.8%.

For neomangiferin-ZIF-8, C1s, N1s, O1s, and Zn2p are located at 284.6, 398.8, 531.6, and 1021.6 eV with atomic percentages of 67.8%, 18.9%, 4.5% and 8.8%.

Fig. S5. DSC-TGA curves of neomangiferin-ZIF-8 (A) and ZIF-8 (B).

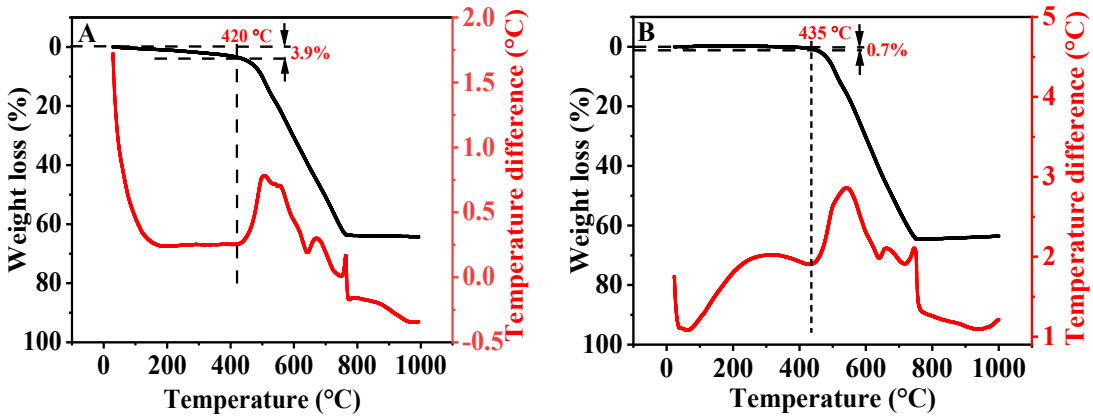

Fig. S6. PXRD patterns of neomangiferin-ZIF-8 before and after sensing in H_2O, MeOH, EtOH, *n*-BuOH, CH_2Cl_2, EA, THF, dioxane, and *n*-hex for 12 h, DMSO for 6 h.

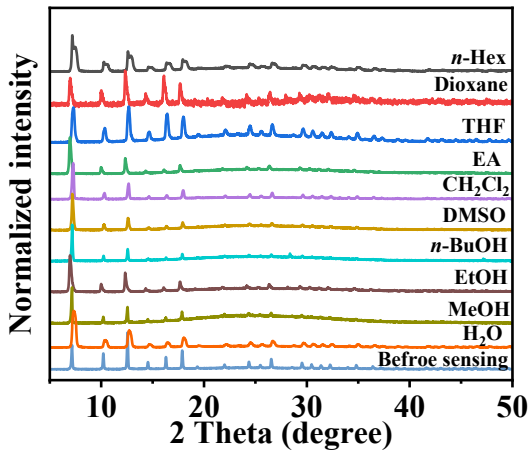

Fig. S7. (A) Fluorescence intensity of neomangiferin-ZIF-8 (1.0 mg/mL) in NaCl solution with different concentrations ($c_{(NaCl)}$, 0−1.0 M); (B) Fluorescence intensity of neomangiferin-ZIF-8 storage for 4 weeks at vacuum dryer (being measured at a concentration of 1.0 mg/mL).

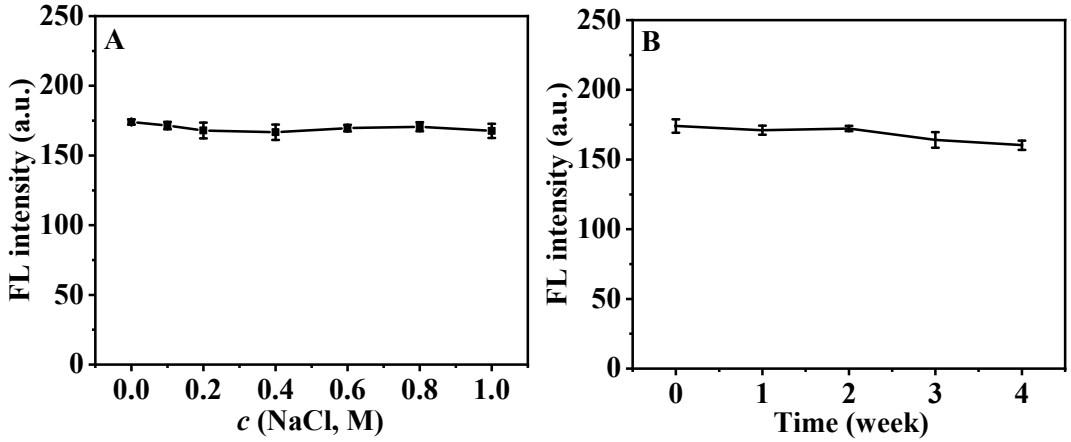

Fig. S8. The excitation and emission spectra of ZIF-8 (A), neomangiferin (B), neomangiferin +Zn^{2+} (C), neomangiferin + MIM (D), and neomangiferin + ZIF-8 (E) (Insets in a and b are the photographs of ZIF-8 and neomangiferin under 365 nm UV light illumination).

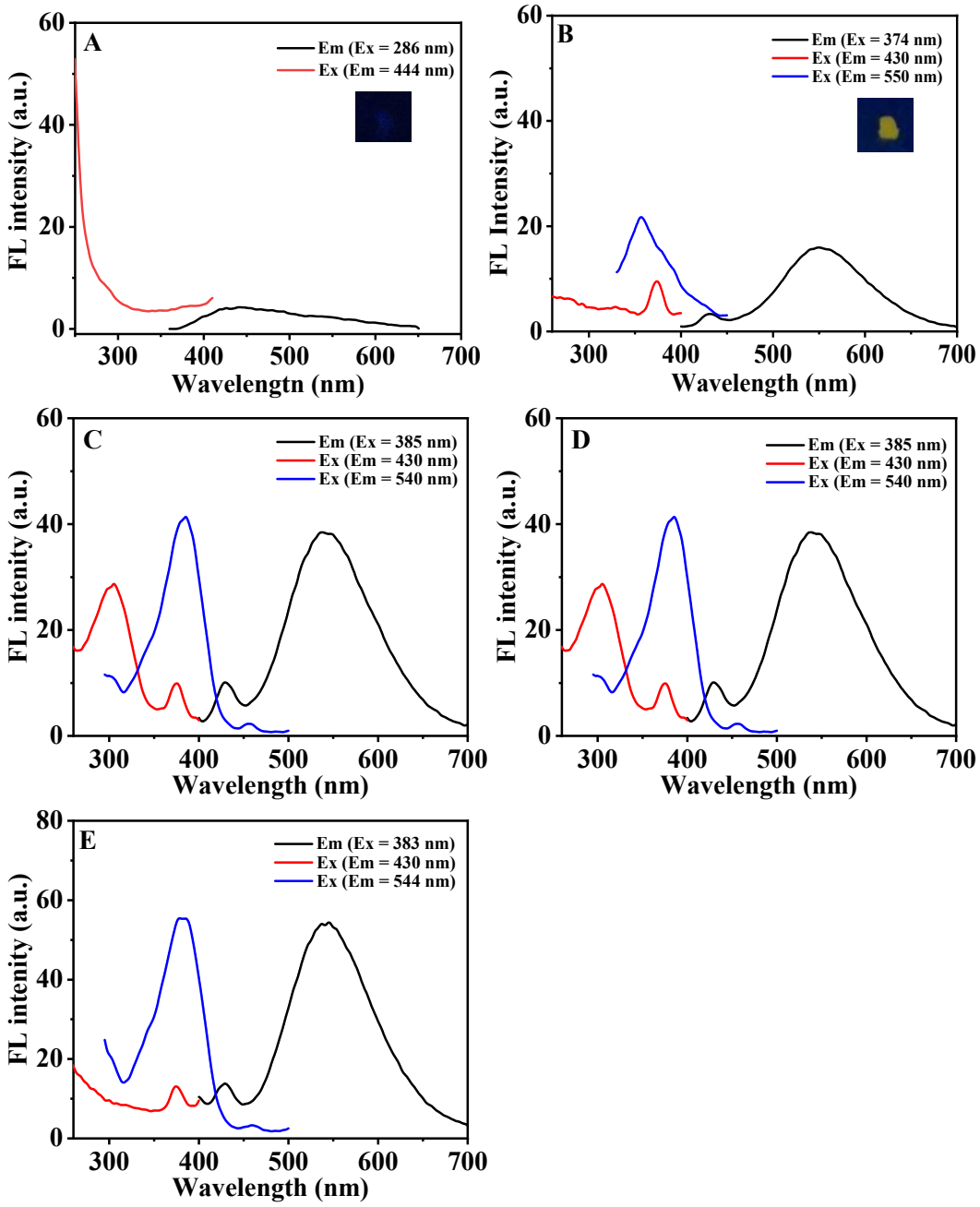

Emission peaks at 430 and 550 nm are for neomangiferin monomer and dimer. The Em for addition of Zn^{2+} are obviously different from those of neomangiferin or neomangiferin-ZIF-8. And the addition of MIM or ZIF-8 seldom changes the maximum emission peaks of neomangiferin.

Fig. S9. The liner relationships between emission peak and E_T^N of solvents by neomangiferin-ZIF-8 synthesized with different molar ratios of Zn^{2+}/MIM.

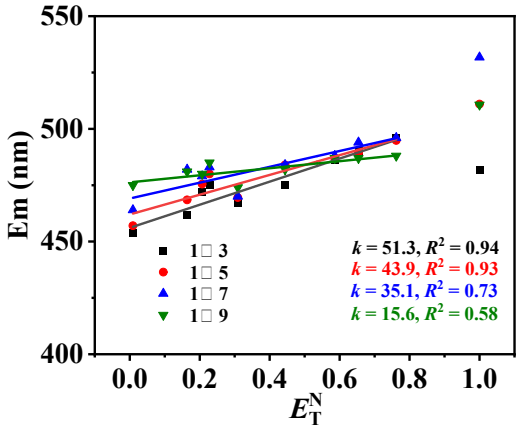

Neomangiferin (4.0 mg) was mixed with $Zn(NO_3)_2 \cdot 6H_2O$ solution (30.0 mM in 20.0 mL of MeOH), and dispersed for 10 min. Next, 20.0 mL of MIM (90.0, 150, 210, or 270 mM in MeOH) was added slowly under stirring. Reaction was carried out at room temperature for 24 h. The molar ratios of Zn^{2+}/MIM were 1:3, 1:5, 1:7 or 1:9. Obviously, neomangiferin-ZIF-8 with Zn^{2+}/MIM molar ratio at 1:3 presents the best solvatochromic behavior. At this reaction system, the final concentrations for Zn^{2+}, MIM, and neomangiferin were 15.0 mM, 45 mM, and 100 μg/mL. The emission peak neomangiferin-ZIF-8 (1:3) increases with the increased polarity indicator value (E_T^N) of solvents with the highest slop (k, 51.3) and the best linear correlation (R^2, 0.94).

Fig. S10. Photographs of solvent-free neomangiferin-ZIF-8 before (A) and after adding 2 μL of EtOH (B) under 365 nm UV illumination.

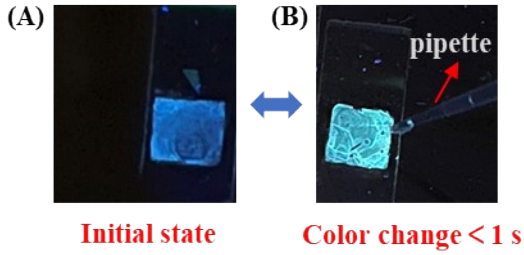

Fig. S11. Normalized fluorescence spectra of neomangiferin (A), ZIF-8 (C) and post-encapsulation neomangiferin@ZIF-8 (E) in different solvents; and the liner relationships between emission peak of neomangiferin (B), ZIF-8 (D) and post-encapsulation neomangiferin@ZIF-8 (F) and E_T^N of solvents.

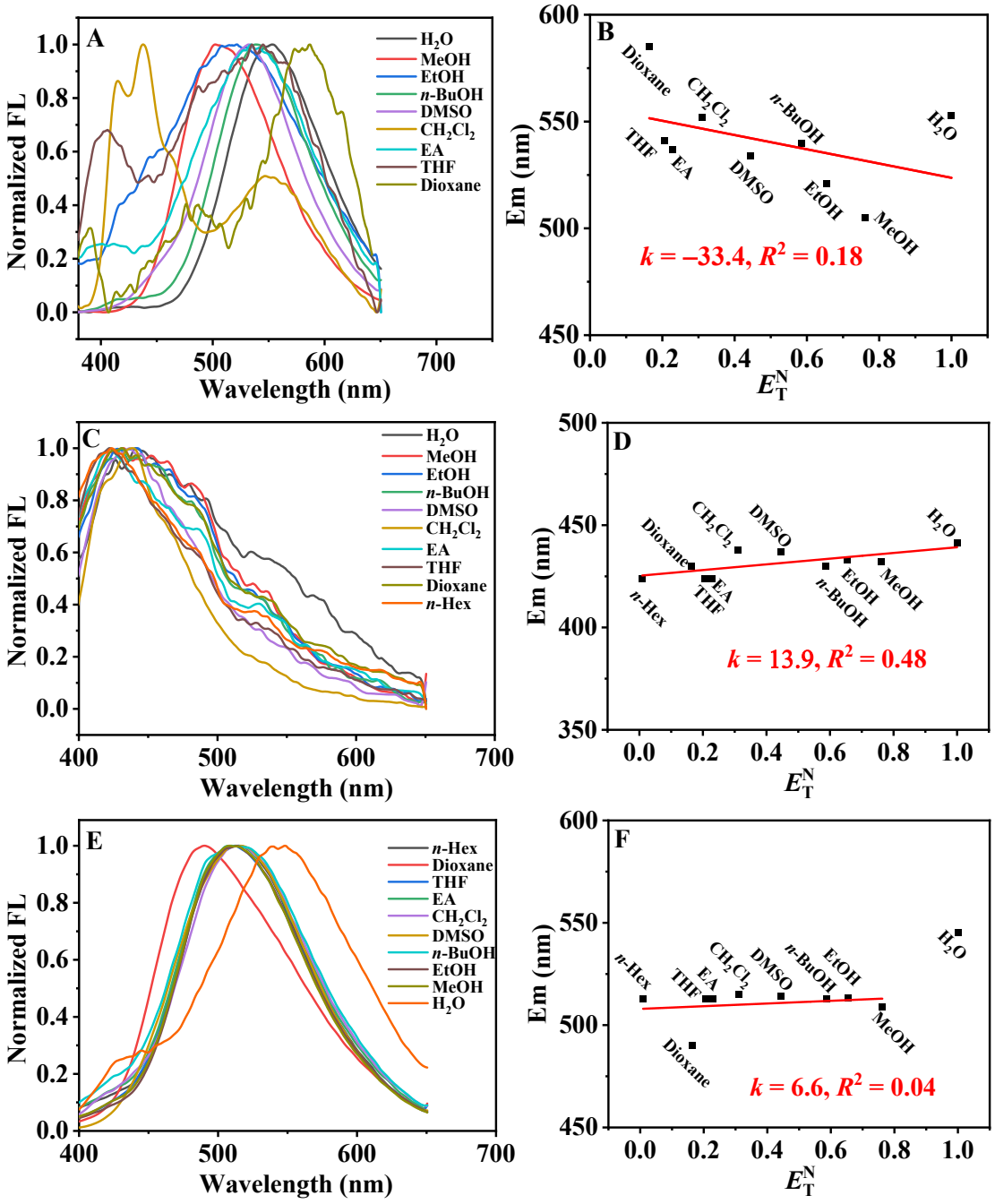

The post-encapsulation of neomangiferin@ZIF-8 was synthesized by mixing the ZIF-8 and neomangiferin (4.0 mg) into 40.0 mL methanol, and stirring under room

temperature for 24 h. Then the product was washed with MeOH for 10 times, dried, and stored in vacuum for further use.

Neomangiferin is insoluble in *n*-hex, thus the date in *n*-hex was not shown. It can be observed from the results (Fig. S11A–B) that neomangiferin is insensitive to the solvent polarity. Solvents can directly react with framework or exchange with coordinated ligands to influence the luminescent property of LMOFs. However, for ZIF-8 and post-encapsulation neomangiferin@ZIF-8, the small slopes (13.9 for ZIF-8 and 6.6 for post-encapsulation neomangiferin@ZIF-8) of fitted linear between Em and E_T^N and the poor linearly dependent coefficients (0.48 for ZIF-8 and 0.04 for post-encapsulation neomangiferin@ZIF-8) imply that their emission peak is almost stable in solvents with different polarity (Fig. S11C–F).

Fig. S12. UV-vis spectra (A) and fluorescence spectra (B, detection voltage at 700 V) of neomangiferin-ZIF-8 in different solvents.

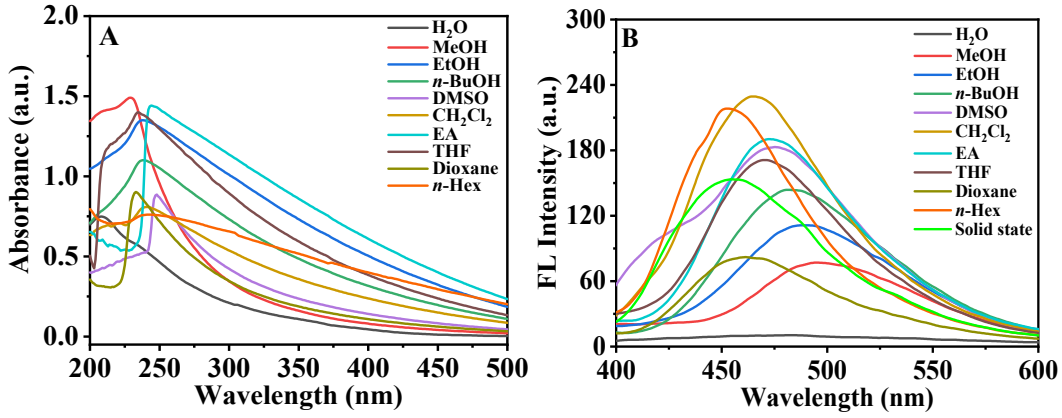

Fig. S13. Fluorescence lifetime decay curve for neomangiferin-ZIF-8 in H_2O.

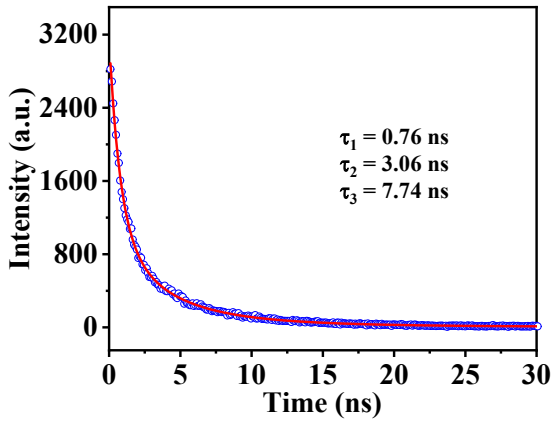

Lifetime data was collected upon exciting at 348 nm. Lifetime data was fitted using triexponential function (R^2 = 0.9990):

$$y = A_1\exp\left(-\frac{t}{\tau_1}\right) + A_2\exp\left(-\frac{t}{\tau_2}\right) + A_3\exp\left(-\frac{t}{\tau_3}\right) + y_0$$

Fig. S14. The F/F_0 value of neomangiferin-ZIF-8 under different incubation time in dioxane with 2.00% (*v*/*v*) of water (A) and in EtOH with 3.00% (*v*/*v*) of water (B).

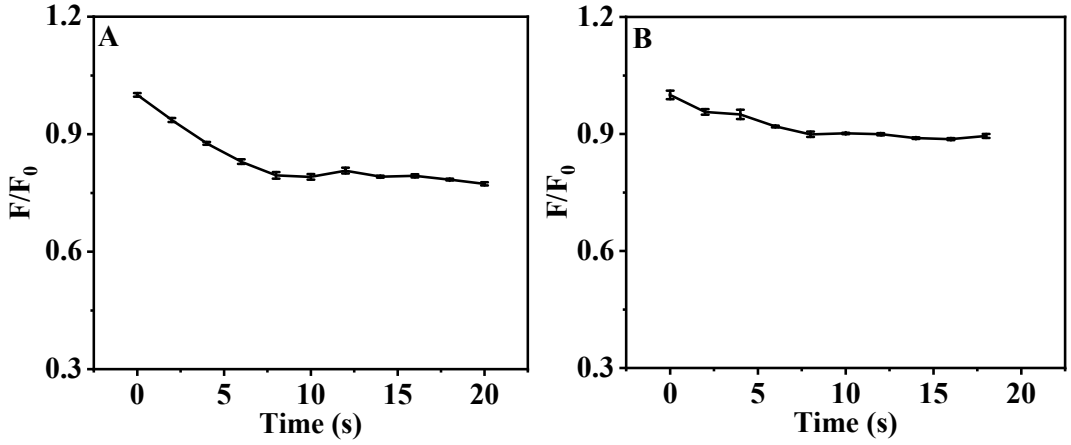

Fig. S15. Fluorescent spectra of neomangiferin-ZIF-8 dispersed in THF (A), DMSO (C), and MeOH (E) with different water contents; Fitting curve between F/F_0 and water content (*v*/*v*, %) in THF (B), DMSO (D), and MeOH (F).

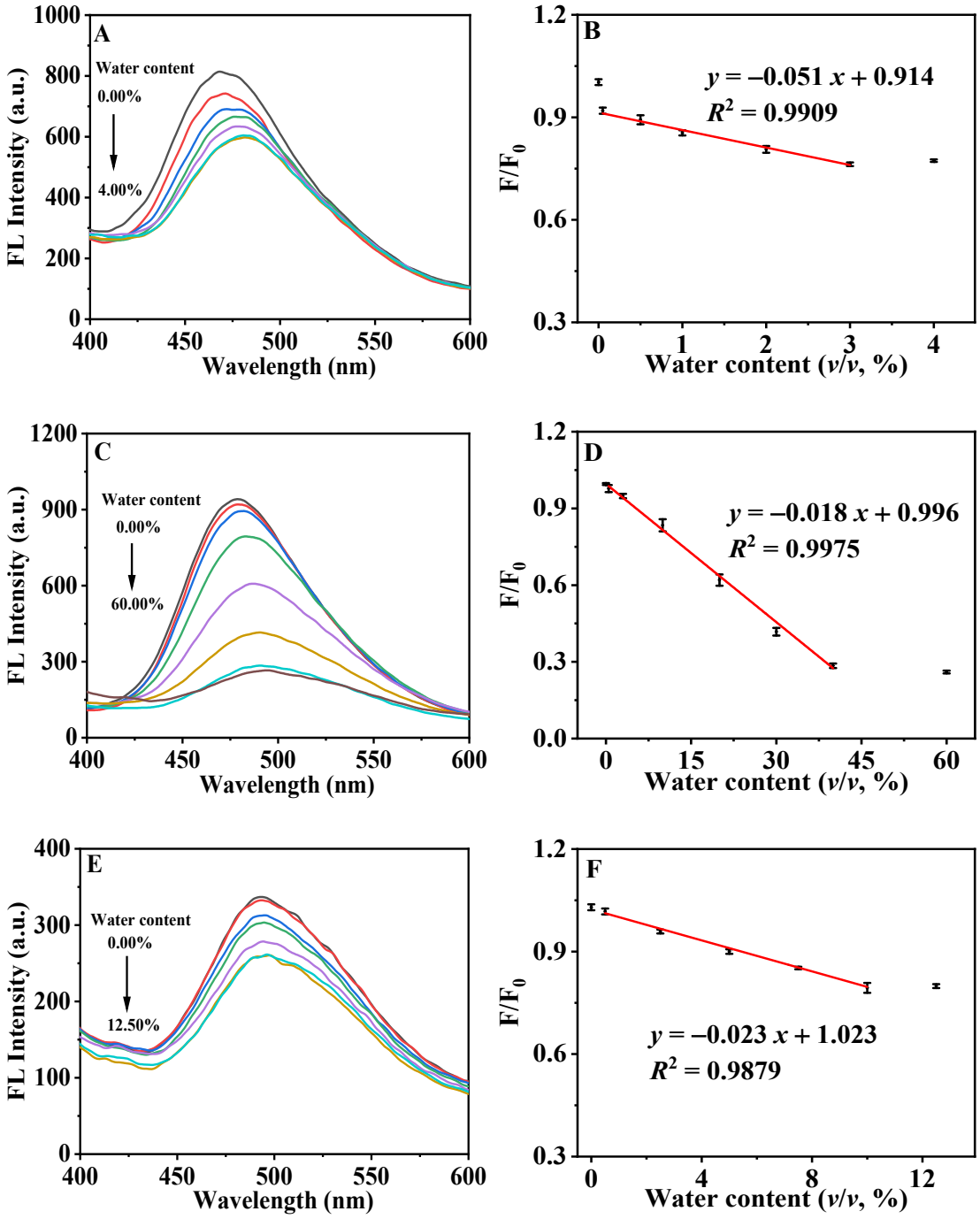

Fig. S16. (A) Fluorescent intensity of neomangiferin-ZIF-8 in CO_2, N_2, CO, H_2, CH_4, O_2, C_2H_6, C_2H_4, C_2H_2, under vacuum and RH of 43.2%; (B) Reversible emission peak change and fluorescent photographs of neomangiferin-ZIF-8 between vacuum and 43.2% RH.

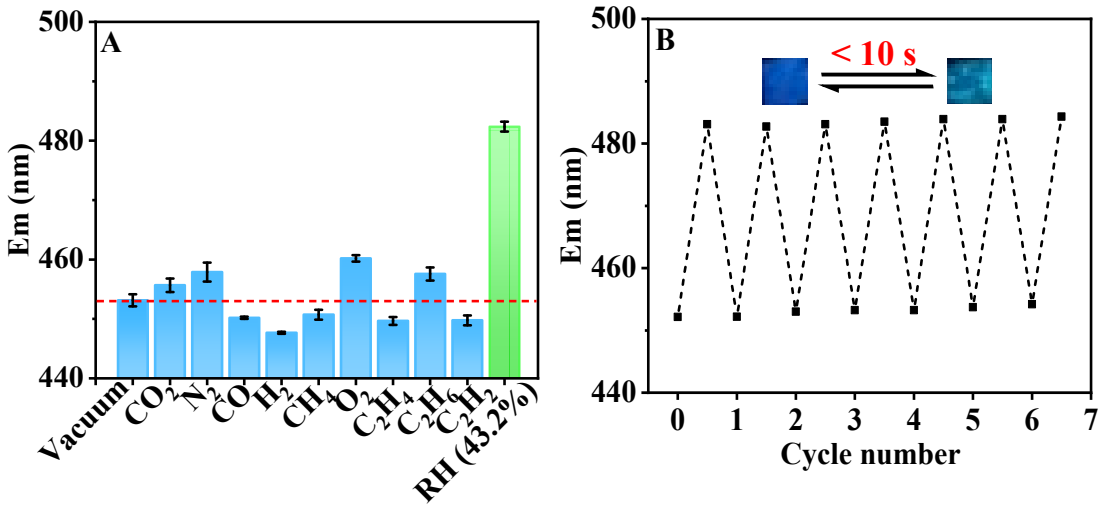

Fig. S17. PXRD patterns of neomangiferin-ZIF-8 before and after sensing of RH (43.2%) for six cycles.